Geophysical Research Letters

RESEARCH LETTER
10.1029/2021GL094532

Winter Euro-Atlantic Climate Modes: Future Scenarios From a CMIP6 Multi-Model Ensemble

E. Cusinato[1], A. Rubino[1], and D. Zanchettin[1]

[1]Department of Environmental Sciences, Informatics and Statistics, University Ca' Foscari of Venice, Venice, Italy

Key Points:

- Euro-Atlantic climate modes are evaluated in CMIP6 *historical* and *ssp585* ensembles using a box-based method for climate index definition
- Models robustly simulate observed spatial patterns of Euro-Atlantic modes, including their impacts on Mediterranean temperature and precipitation
- The *ssp585* ensemble indicates non-significant trends in NAO, EAWR, and SCA, and a progression toward a persistent positive phase of EA

Supporting Information:

Supporting Information may be found in the online version of this article.

Correspondence to:

E. Cusinato,
eleonora.cusinato@unive.it

Citation:

Cusinato, E., Rubino, A., & Zanchettin, D. (2021). Winter Euro-Atlantic climate modes: Future scenarios from a CMIP6 multi-model ensemble. *Geophysical Research Letters*, *48*, e2021GL094532. https://doi.org/10.1029/2021GL094532

Received 25 MAY 2021
Accepted 17 SEP 2021

Author Contributions:

Conceptualization: D. Zanchettin
Data curation: E. Cusinato
Formal analysis: E. Cusinato, A. Rubino, D. Zanchettin
Methodology: E. Cusinato, D. Zanchettin
Writing – original draft: E. Cusinato, A. Rubino, D. Zanchettin
Writing – review & editing: E. Cusinato, A. Rubino, D. Zanchettin

Abstract Dominant Euro-Atlantic modes of large-scale atmospheric variability significantly affect interannual-to-decadal Euro-Mediterranean climate fluctuations, especially in winter. Here, we investigate the robustness of historical and projected state and variability of such modes in a CMIP6 multi-model ensemble of *historical* and *ssp585* future scenario simulations, focusing on the winter season. Results show overall good skills of the *historical* ensemble to reproduce the observed temporal, spectral and distributional properties of all considered modes. At the end of the 21st Century the *ssp585* ensemble yields non-significant distributional changes for NAO, EAWR, and SCA indices and a transition to a baroclinic structure for EA, with persistent positive anomalies in the mid-troposphere enhancing globally-driven warming over the Euro-Mediterranean region. The hemispheric spatial correlation patterns with temperature and precipitation significantly change for all modes, that is, we observe a significant modulation of the teleconnections associated with each index.

Plain Language Summary Modes of variability in the large-scale atmospheric circulation over the Euro-Atlantic region are evaluated in a multi-model ensemble of simulations contributing to the sixth phase of the Coupled Model Intercomparison Project (CMIP6) under historical conditions and under a projected future global warming scenario. The modes' key features in the winter season are analyzed in terms of temporal, spectral and distributional properties. Results show that overall CMIP6 models reproduce well the observed properties. The mode known as Eastern Atlantic pattern (EA) is projected to change substantially in the course of the 21st Century above the boundary layer, where the EA index evolves toward persistent positive values. As a positive EA is associated with anomalous warming over Europe, this contributes to enhancing the projected globally-driven warming.

1. Introduction

Especially during winter, the North Atlantic Oscillation (NAO), the Eastern Atlantic pattern (EA), the Eastern Atlantic Western Russian pattern (EAWR) and the Scandinavian pattern (SCA) are dominant modes of Euro-Atlantic atmospheric variability. They are associated with large-scale patterns of tropospheric pressure and circulation anomalies that can last for several weeks or months, and sometimes even years (Hurrell et al., 2003), and significantly affect interannual-to-decadal climatic and hydroclimatic variability in the Euro-Mediterranean region over spatial patterns that are specific for each mode (e.g., Cusinato et al., 2019; Marshall et al., 2001; Zanchettin et al., 2008). NAO, EA, EAWR, and SCA are originated by a host of different processes including ocean-atmosphere interactions (e.g., Bellucci et al., 2008), stratosphere-troposphere coupling (e.g., Perlwitz & Graf, 1995; Shaw & Perlwitz, 2013; Thompson et al., 2003) and wavelike atmospheric dynamics (e.g., Bueh & Nakamura, 2007; Lim, 2015; Woollings et al., 2008). The observed temporal evolution of these modes show that, beyond interannual variability, their prominent historical features include a positive trend component for NAO from 1950 to the mid-1990s, possibly forced by atmosphere-ocean interactions (Hoerling et al., 2001; Raible et al., 2005; Schneider et al., 2003), a strong and persistent positive trend component for EA during 1997–2004, and lack of significant trend for EAWR and SCA (NOAA—Climate Prediction Center).

However, how these modes are expected to respond to changing global climate conditions remains rather unexplored. Here, we tackle this question by analyzing a multi-model ensemble of state-of-the-art historical and future global-warming scenario climate simulations.

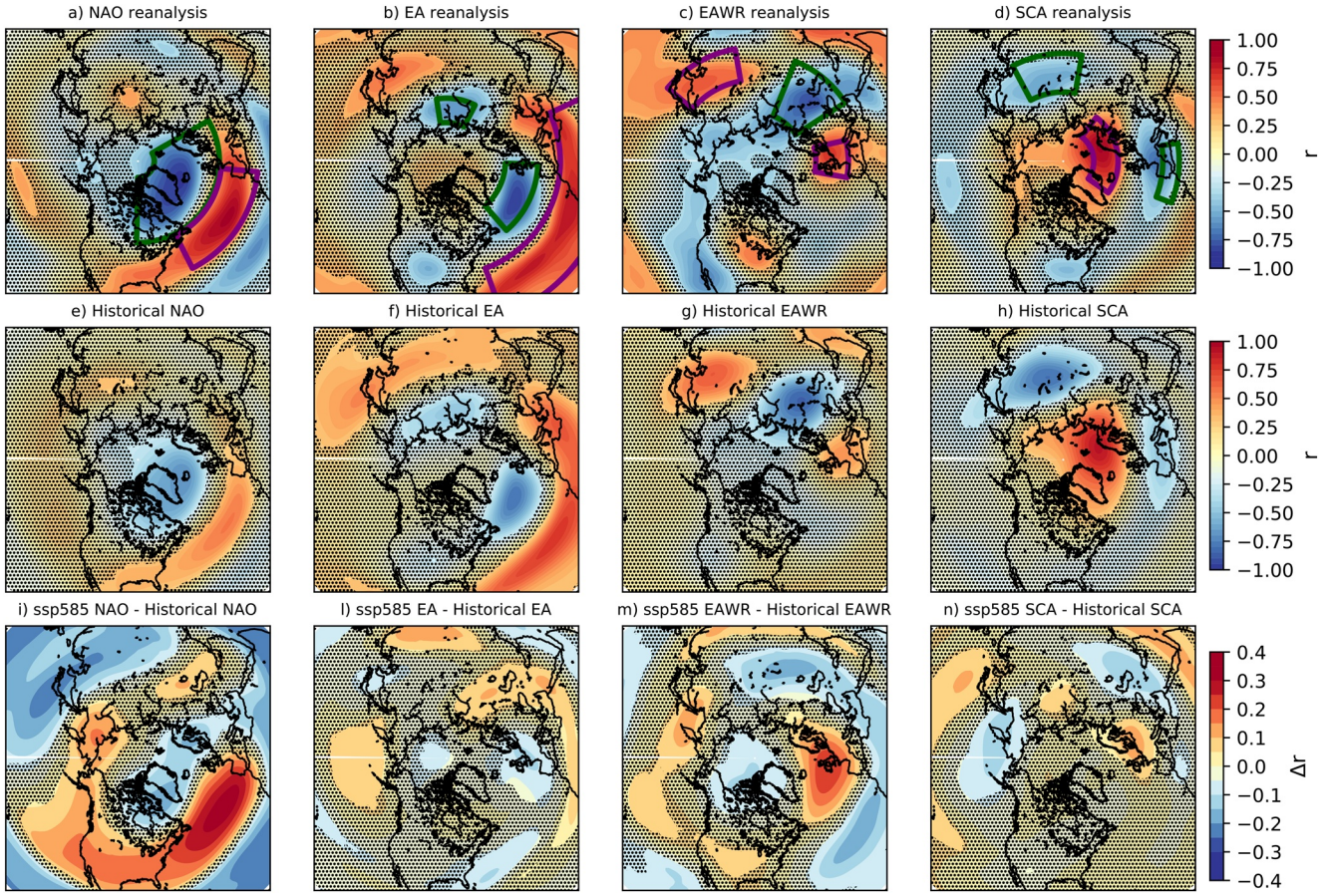

Figure 1. Spatial patterns of NAO, EA, EAWR, and SCA. (a–d) Correlation maps between gridded winter Z500 anomalies and the considered indices for the ERA-Interim reanalysis (1980–2014); (e–h) Ensemble-mean correlation maps between gridded winter Z500 anomalies and the considered indices for the *historical* simulations (1960–1999). (i–n) Ensemble-mean difference between correlation maps for the *ssp585* (2060–2099) and the *historical* simulations. In all panels, black dots illustrate statistical non-significance (see methods). Colored boxes in panels (a–d) indicate the boxes encompassing the action centers of each mode (green: negative centers; purple: positive centers). All data were linearly detrended before analysis.

The typical spatial structure of NAO, EA, EAWR, and SCA is characterized by dipoles or triple poles of teleconnected anomalous atmospheric pressure centers, which are located over the North Atlantic for NAO and EA, and over Scandinavia and Eurasia for SCA and EAWR (Figures 1a–1d). Shifts in their location occur on decadal and interdecadal timescales over the North Atlantic sector (e.g., for the NAO: Raible et al., 2014), reflecting variations in the atmospheric pressure anomalies linked with basin-scale sea-surface temperature variability (e.g., Bjerknes, 1964). Nevertheless, a paradigm assuming stationary teleconnections is used, which allows to easily define indices for these modes: Their positive and negative phases are then associated with strengthened and weakened patterns, respectively (e.g., NOAA—Climate Prediction Center). Analysis of the indices' evolution reveals significant interannual-to-decadal variability associated to these modes, which for NAO and EA extends even to multi-decadal variability (e.g., Barnston and Livezey, 1987; Bracegirdle et al., 2018; Zanchettin et al., 2009).

In the context of multi-model analyses only the NAO has been extensively studied, especially concerning future scenarios (e.g., Bracegirdle et al., 2018; Davini & Cagnazzo, 2014; Ning & Bradley, 2016; Wang et al., 2017), whereas few studies focused on the remaining climate modes (e.g., Casado & Pastor, 2012). This study fills this gap of knowledge by investigating the presence of robust changes in NAO, EA, EAWR, and SCA in multi-model ensembles of *historical* simulations and simulations under the *ssp585* future scenario of anthropogenic forcing (corresponding to a fossil-fueled development with 8.5 W/m^2 forcing level) performed in the frame of the sixth phase of the Coupled Model Intercomparison Project (CMIP6, Eyring et al., 2016).

The study aims at answering the following scientific questions: How do CMIP6 climate models simulate observed features of winter NAO, EA, EAWR, and SCA? How are the simulated temporal, spectral and distributional properties of these modes affected by future global warming conditions?

2. Materials and Methods

2.1. Box-Based Indices

Indices for each climate mode are defined following an updated version of the box method approach (Stephenson et al., 2006; Wallace & Gutzler, 1981). This method considers identifiable and stationary centers of actions. The index is obtained by a linear combination of anomalies in such centers of action. This method is preferred here to alternative approaches (e.g., those based on empirical orthogonal functions) since it provides for a univocal definition of the index across sources (namely observations and models) and avoids embedding uncertainties linked to the variable covariance structure of the spatio-temporal data (e.g., Raible et al., 2014; Zanchettin et al., 2016) in a multi-model framework where different models and multiple simulations with the same model are considered. This new procedure for the indices definition is explained in detail in Text S1 in Supporting Information S1; in general for each mode the box-based index is calculated using winter-average (December–February) time series of 500 hPa geopotential heights (Z500) anomalies obtained from the ERA-Interim reanalysis for the period 1980–2014 as follows. Centers of action and seed boxes are identified based on a regression of the gridded Z500 anomalies (deviations from the 1980–2014 climatology) on the target index provided by the Climate Prediction Center of the NOAA. Then a set of boxes is obtained by translations and stretching of the seed box for each center of action. The combination of boxes yielding the highest correlation between the box-based and NOAA indices is retained. The shapes of the final boxes for each index are illustrated in Figures 1a–1d, while Table S1 in Supporting Information S1 reports their geographical coordinates. The equations to calculate the indices are:

$$\mathrm{NAO} = -8.57 \times 10^{-5} - 0.015 \cdot \mathrm{neg1} + 0.017 \cdot \mathrm{pos1}, \quad (1)$$

$$\mathrm{EA} = -0.005 \cdot \mathrm{neg1} - 0.009 \cdot \mathrm{neg2} + 0.054 \cdot \mathrm{pos1}, \quad (2)$$

$$\mathrm{EAWR} = 2.857 \times 10^{-5} - 0.021 \cdot \mathrm{neg1} + 0.010 \cdot \mathrm{pos1} + 0.007 \cdot \mathrm{pos2}, \quad (3)$$

$$\mathrm{SCA} = -5.714 \times 10^{-5} - 0.013 \cdot \mathrm{neg1} + 0.003 \cdot \mathrm{neg2} + 0.016 \cdot \mathrm{pos1}, \quad (4)$$

where pos* and neg* represent boxes for centers of action characterized by positive and negative Z500 anomalies, respectively. The approach improves the original box-based method by Wallace and Gutzler (1981) in that shape and weight of each center of action are not set *a priori* but identified through a statistical-based optimization procedure. These equations and their corresponding boxes (see Table S1 in Supporting Information S1) are used to compute indices for the simulations contributing to the multi-model ensemble. We therefore used fixed boxes for the indices definition in CMIP6 simulations, assuming that the centers of action of the considered modes do not change their spatial characteristics and relative weight for the index in the *historical* and *ssp585* scenario conditions.

The same box-based method is also used to compute NAO, EA, EAWR, and SCA indices based on the sea-level pressure (SLP) field, so that the analysis is performed both in the mid-troposphere and at the surface.

2.2. Statistical Analyses

Wintertime series of NAO, EA, EAWR, and SCA indices are computed for each simulation using Equations 1–4 and then standardized over the period 1980–2014.

Analyses are performed on two reference periods: 1960–1999 for the *historical* and 2060–2099 for the *ssp585* simulations. Changes in the empirical distribution of the indices under *historical* and *ssp585* conditions are visualized using a combination between boxplots and Kernel density function estimates (violinplots: Hintze & Nelson, 1998). The Mann-Whitney U test is used to identify significant differences ($p < 0.05$) between

the *historical* and *ssp585* distributions: As a null hypothesis we state no distributional difference between *historical* and *ssp585* ensembles.

Empirical power spectral density is estimated for each index and each realization using the Welch method (Welch, 1967). The median and the 5th and 95th percentiles for the *historical* and the *ssp585* ensembles are used to illustrate expectation and envelope of the ensemble spectral density estimates, respectively.

The spatial signature of each mode on winter Z500, near-surface air temperature and precipitation is illustrated using maps of gridded Pearson's correlation coefficients between linearly detrended time series of paired index and physical variable. For ensemble results, these coefficients are calculated for each simulation on the corresponding model grid and then spatially bilinearly interpolated to a common grid ($1° \times 1°$). The ensemble signature is considered robust where at least half of the simulations yield a statistically significant ($p = 0.05$) local correlation. Differences between spatial patterns of the *historical* and *ssp585* ensembles are evaluated using the Mann-Whitney U test applied to local correlation coefficients.

3. Data

3.1. The CMIP6 Multi-Model Ensemble

We use output (winter monthly averaged Z500, SLP, near-surface air temperature and precipitation) from 24 CMIP6 models (Table 1). The ensemble comprises *historical* simulations from 1851 to 2014 and associated *ssp585* simulations from 2015 to 2099. Multiple realizations (r1i1p1f1, r2i1p1f1, and r3i1p1f1) are considered for some models based on availability.

4. Results

4.1. Historical Observations and Simulations

Figure 1 illustrates the spatial pattern of the four indices for the reanalysis and the ensemble simulations. The similarity of patterns in panels (a–d) and (e–h) indicates that for all modes the multi-model ensemble captures the shape of the centers of action and the magnitude of their teleconnection, slightly underestimating especially the negative centers. The ensemble agreement drops substantially outside the boxes used to construct each index, with only a few regions displaying robust results across models. For instance, there is a robust positive signature of the NAO over the Southeastern US and a robust positive signature of the EA over the exit region of the East Asian jet stream.

The multi-model ensemble captures well the associated observed temperature pattern (Figure S1 in Supporting Information S1), except for the EA showing positive correlation over the south-eastern Asia and the western North Atlantic. All indices but SCA are positively correlated with temperature over central Asia. Regarding precipitation (Figure S2 in Supporting Information S1), simulations robustly reproduce the observed positive correlations over the Atlantic for NAO and EA and over Asia for EA and EAWR, and the observed negative correlations over Asia for SCA.

Figure 2 illustrates the *historical* and *ssp585* ensemble time-series of the four indices and their spectral characteristics. The *historical* ensemble agrees with the observed evolution of the indices with a very few exceptions. The observed positive trend in the EA emerges also in the ensemble-mean, although weaker in the simulations, suggesting that it stems partly from a forced response. There are anomalies in the ensemble-mean of EA and NAO that correspond to periods of major volcanic activity (e.g., around the 1883 Krakatau and the 1991 Pinatubo eruptions), highlighting the sensitivity of these modes to external forcing (e.g., Zanchettin et al., 2012). Otherwise, the simulated indices show a remarkable stability in the mean state over the whole historical period. Observed indices show specific timescales of variability, while there is no robust occurrence of such periodicities in the multi-model ensemble (Figures 2e–2h) and, for all modes, the ensemble envelope contains the observed spectrum. Therefore, preferred timescales of interannual-to-decadal variability for these modes do not exist, in agreement with the classical stochastic climate models such

Table 1
List of CMIP6 Models Used to Perform the Multi-Model Ensemble Analyses

Institution	Model	Simulations (*historical* and *ssp585*)			Reference	Simulation name in this paper
		r1i1p1f1	r2i1p1f1	r3i1p1f1		
CSIRO (Australia)	ACCESS-CM2	X	X	X	Bi et al. (2020)	CSIROCM2-1/2/3
	ACCESS-ESM1-5	X	X	X	Ziehn et al. (2020)	CSIROESM2-1/2/3
AWI (Germany)	AWI-CM-1-1-MR	X			Semmler et al. (2020)	AWICM-1
BCC (Beijing, Asia)	BCC-CSM2-MR	X			Wu et al. (2019)	BCCCSM2-1
CAMS (China)	CAMS-CSM1	X	x		Rong et al. (2019)	CAMSCSM-1/2
NCAR (USA)	CESM2-WACCM	X	x	X	Danabasoglu et al. (2020)	CESM2WACCM-1/2/3
CMCC (Italy)	CMCC-CM-SR5	X			Cherchi et al. (2019)	CMCCCM2-1
CCCma (Canada Climate Center)	CanESM5	X	x	X	Swart et al. (2019)	CanESM5-1/2/3
EC-Earth-Consortium (Europe)	EC-Earth3	X			Massonnet et al. (2020)	ECEarth3-1
	EC-Earth3-Veg	X	x	X	Wyser et al. (2020)	ECEarth3Veg-1/2/3
CAS (China)	FGOALS-f3-L	X			He et al. (2019)	FGOALSf3-1
	FGOALS-g3	X	x	X	Li et al. (2020)	FGOALSg3-1/2/3
FIO (China)	FIO-ESM2	X	x	X	Song et al. (2019)	FIOESM2-1/2/3
NOAA-GFDL (USA)	GFDL-ESM4	X			Dunne et al. (2020)	GFDLESM4-1
CCR-IITM (India)	IITM-ESM	X			Krishnan et al. (2019)	IITMESM-1
INM (Russia)	INM-CM4-8	X			Volodin et al. (2018)	INMCM4-1
IPSL (France)	IPSL-CM6A-LR	X	x	X	Boucher et al. (2020)	IPSLCM6A-1/2/3
MIROC (Japan)	MIROC6	X	x	X	Tatebe et al. (2019)	MIROC6-1/2/3
MPI (Germany)	MPI-ESM1-2-HR	X	x		Müller et al. (2018)	MPIESMHR-1/2
	MPI-ESM1-2-LR	X	x	X	Müller et al. (2018)	MPIESMLR-1/2/3
MRI (Japan)	MRI-ESM2-0	X			Yukimoto et al. (2019)	MRIESM2-1
NCC (Norway)	NorESM2-LM	X			Seland et al. (2020)	NorESM2LM-1
	NorESM2-MM	X			Seland et al. (2020)	NorESM2MM-1
AS-RCEC (Thailandia)	TAIESM1	X			Lee et al. (2020)	TAIESM1-1

as the local interaction (Hasselmann, 1976) and the propagation (Frankignoul et al., 1997) model. Similar considerations stand for the indices computed over the SLP field (Figure S3 in Supporting Information S1).

4.2. The *ssp585* Scenario

Figures 2a–2d show the continuation of the simulated evolution of the considered indices to the end of the 21st Century under the *ssp585* scenario. The multi-model ensemble yields no robust change in the mean state of NAO and SCA, which also display no significant change in their variance. EAWR undergoes a slight negative change in the mean state with an increase in the variance, while EA features a large and robust change in the mean state evident as a positive trend, and a substantial increase in variance. At the end of the *ssp585* simulations the EA ensemble-mean values reach around +5 standard deviations. In contrast, no change in the mean state is identified in any index in the *ssp585* compared to the *historical* simulations for the SLP-based indices (Figure S3 in Supporting Information S1). Analysis of EA changes across all model levels (Figure S4 in Supporting Information S1) demonstrates a transition of the vertical structure of the EA from an almost barotropic to a marked baroclinic structure that reveals the different response of associated mid-troposphere and surface processes to global warming.

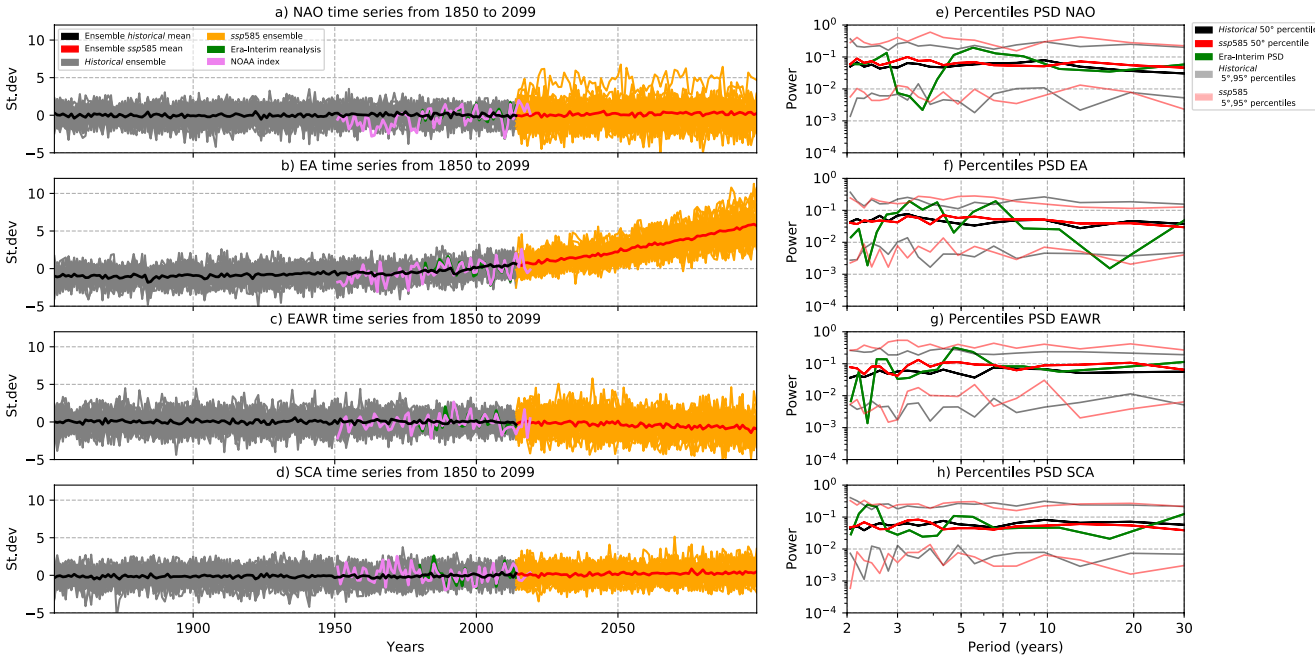

Figure 2. Temporal and spectral characteristics of the modes. (a–d) Time-series of winter NAO, EA, EAWR, and SCA indices (gray/black: *historical* individual simulations/ensemble mean, orange/red: *ssp585* individual simulations/ensemble mean, violet: NOAA, green: reanalysis). Standardization is over the period 1980–2014. (e–h) Power spectral density (PSD) of the indices (green: reanalysis, black: *historical* simulations for period 1960–1999; red: *ssp585* simulations for period 2060–2099). The 5th, 50th (thick line) and 95th percentiles are shown for each ensemble.

To illustrate the implications of these changes in terms of distributional properties and inter-model differences, Figure 3 shows violinplots of the indices calculated for each of the *historical* (1960–1999) and *ssp585* (2060–2099) simulation separately. The figure confirms the significant and pronounced positive shift in the *ssp585* distribution of EA compared to *historical* conditions. For most simulations both distributions do not

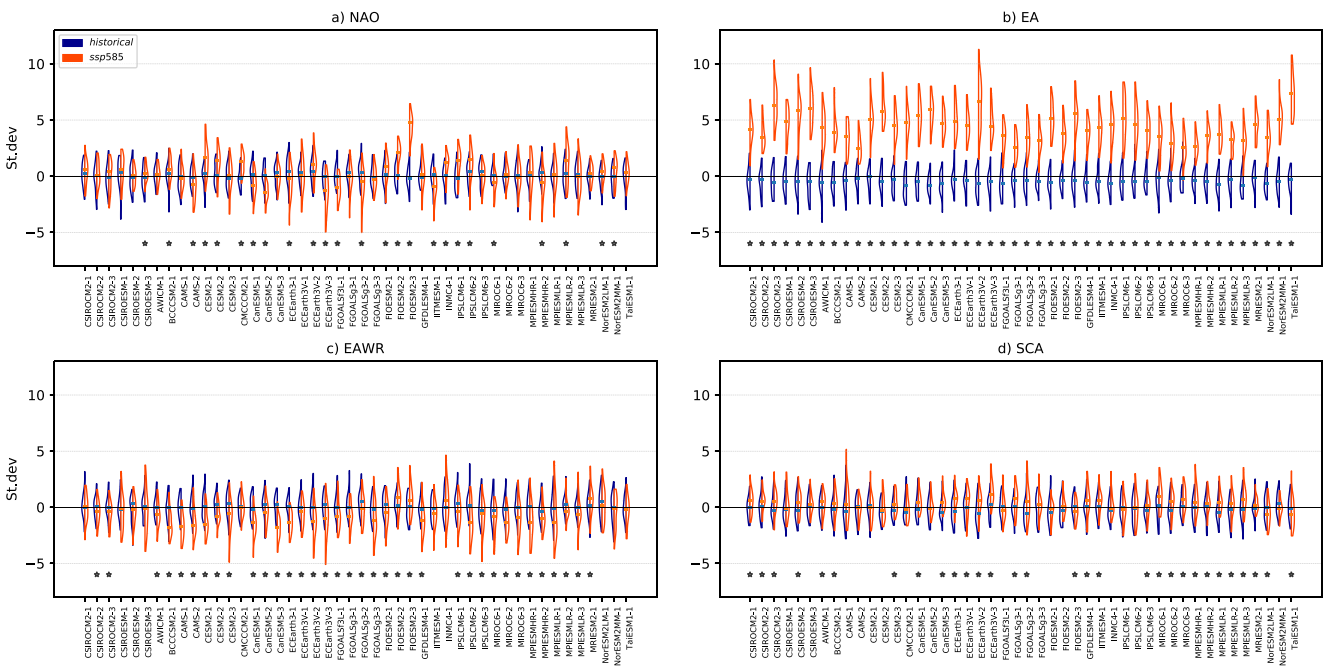

Figure 3. Violinplots of (a) NAO, (b) EA, (c) EAWR and (d) SCA indices from the individual *historical* (1960–1999) and *ssp585* (2060–2099) simulations. Significant differences between the distributions of the *historical* and the associated *ssp585* simulations are highlighted by asterisks.

overlap. In some cases, as for the ECEarth3V-2 and the CSIROESM-2 simulations, the shift is associated with an increase in variance. However, different realizations within the same models do not display this feature.

For the EAWR most simulations show a significant negative shift in the *ssp585* distribution compared to *historical* conditions with the exception of FIOESM2-2, FIOESM2-3 and MRIESM2-1, and overall both distributions overlap. The shift is associated with an increase in variance only in some cases, as for the CESM2-3, ECEarth3V-3 and MPIESM12LR-1 simulations.

For the NAO the ensemble displays overall no robust changes in the distributional properties, and occasional significant changes disagree in the sign (see CESM2-1 and FGOALSf3L-1, FIOESM2-3 and IITMESM-1). Changes are even less appreciable and coherent for the SCA, where the subset of models showing significant changes indicate a shift toward negative values, for instance FIOESM2-3, NorESM2LM-1 and TaiESM1-1.

Figures 1i–1n display the difference between the spatial patterns of the modes in the *ssp585* ensemble and the corresponding *historical* ones. As the spatial patterns are illustrated as correlation maps, the difference reveals changes in the teleconnections due to interannual variability of the index, beyond changes in the mean.

The anomalous correlation pattern of NAO largely superposes on its *historical* pattern with an extensive robust negative anomalous correlation occurring over the Pacific, the subtropical Atlantic and to the east of the Caspian Sea and a positive anomalous correlation occurring over the North Atlantic, the United States and the North Pacific, which together suggest a stronger circum-global mid-latitude structure of the pattern. Also the anomalous correlation pattern of EA superposes on its *historical* pattern, but it suggests a westward displacement of its centers of action with the negative center extending over Northern Europe and the Bay of Biscay and the positive center extending to the east of the Caspian Sea. For both modes the *ssp585* correlations are lower compared to the *historical* conditions.

The anomalous correlation patterns of EAWR and SCA only partly superpose on their *historical* pattern, implying that simulated robust changes in their teleconnections do not simply concern strengthened or weakened variability in the associated centers of action. The anomalous correlations of SCA suggest a south-westward displacement of the centers of actions with the positive center extending toward the Bay of Biscay. Changes are more complex for the EAWR, which undergoes an eastward displacement of the positive center over China, a weakening and a northern displacement of the positive center over Northern Europe and an extension of the negative center from Asia to southern Europe and Atlantic Ocean.

Changes in the atmospheric teleconnections of the modes under the *ssp585* scenario are associated with changes in their signature on temperature and precipitation (Figures S1 and S2 in Supporting Information S1). For both variables the changes entail overall weaker correlations compared to the *historical* ones for all the modes. EA changes its imprint on temperature and precipitation over Siberia and Eastern Asia, where however the Z500-based index disagrees with observations and the SLP-based index (Figures S5 and S6 in Supporting Information S1). Similar concerns stand for the NAO imprint on precipitation over Siberia and Eastern Asia.

For the EAWR and temperature, significant changes in the imprint over Europe are associated with a reorganization of the mode's influence over the North Atlantic, Europe, Asia and the eastern North Pacific; for precipitation, beyond a general weakening of the imprint over Europe, the limited realism of the simulated patterns prevents conclusive statements beyond the robustness of the simulated changes (e.g., over the Nordic Seas). For the SCA, changes are patchy and partly superpose on the *historical* temperature and precipitation patterns, except for a strengthening of the temperature response over the Baltic Sea.

5. Discussion and Conclusions

Dominant winter Euro-Atlantic climate modes including NAO, EA, EAWR, and SCA were studied in a CMIP6 multi-model ensemble of *historical* and *ssp585* simulations. Box-based indices built on Z500 fields were used to evaluate the ensemble regarding the models' skill to simulate the modes' key observed features and to identify robust simulated changes under a strong future global warming scenario. Overall, CMIP6

models robustly reproduce the observed spatial patterns of all modes and their associated impacts on temperature and precipitation.

The large amount of scientific works literature existing on the NAO demonstrate an important progress in the simulation of this mode through the various CMIP initiatives (see e.g., Bracegirdle et al., 2018; Davini & Cagnazzo, 2014; Ning & Bradley, 2016; Wang et al., 2017). In this sense, our assessment confirms the overall good model skills in representing observed NAO features, with only some minor possible deficiencies regarding the subpolar center.

In contrast to the NAO, only a few multi-model studies focused on EA, EAWR, and SCA. Casado and Pastor (2012) found good skills of CMIP3 models to reproduce the SCA spatial pattern. Our assessment demonstrates that CMIP6 models overall yield realistic EA, EAWR, and SCA, paving the way toward a deeper investigation on these modes.

Our results show that in the *ssp585* scenario NAO, EAWR, and SCA do not change substantially with respect to *historical* conditions, whereas EA evolves toward a persistent positive phase of the index in its mid-troposphere expression together with a weakening of interannual-to-decadal variability. This shift vanishes at near-surface levels yielding a shift from a rather barotropic toward a marked baroclinic structure of the mode. There is a strong agreement across CMIP6 models regarding the projected EA change, which reflects response to the strong forcing assumed in the considered scenario. The changes in the vertical structure of EA and its dynamical connection with external forcing deserve further investigation.

NAO, EA and EAWR are associated with a weakening of their historical spatial pattern under the *ssp585 s*cenario. These changes superimpose on the pattern of climatological changes where global warming is associated with thermal expansion of the lower atmosphere, which impacts the mean geopotential height as observed in the general rise of Z500 during the twentieth Century (e.g., Christidis & Stott, 2015). Geopotential height trends are, however, spatially and seasonally variable, with the rise being especially strong in mid-latitude and polar regions of the winter hemisphere.

The ensemble-mean climatological changes in winter indicate that in the Northern Hemisphere the rise of Z500 is comparatively smaller near Subpolar Lows (Figure S7a in Supporting Information S1). Over the North Atlantic the Z500 changes superpose well with the EA pattern, therefore explaining the evolution toward a persistent positive phase of the associated index. The polar center of action of NAO extends over regions that undergo a strongly differential Z500 evolution, possibly driven by surface dynamics triggered by winter sea-ice reduction and associated ocean heat releases to the atmosphere and consequent warming (Figure S7b in Supporting Information S1). SCA and EAWR simulated responses to global warming could be associated with climatological changes in Arctic sea ice and in the jet stream strength and location, particularly regarding the exit region of the East Asian subtropical jet.

The Euro-Mediterranean region is projected to undergo a ∼2.5–5°C warming and a meridionally asymmetric precipitation response between −10 and −5 mm/month drying over the Mediterranean and between +10 and +15 mm/month over Central and Northern Europe (Figure S7c in Supporting Information S1). The relative role of the radiative and dynamical responses linked to the large-scale circulation in determining regional climate changes can be quantified by confronting the climatological changes (Figure S7 in Supporting Information S1) with the changes in strength and spatial patterns of the modes (Figures S1 and S2 in Supporting Information S1): The climatological pattern of the EA positively superposes on the global warming pattern over Europe, hence the mid-troposphere EA strengthening may contribute to enhance European warming and Mediterranean drying. Such a possibility remains to be further explored.

The found changes in the modes in terms of indices' variations and teleconnection patterns can be fully understood with an assessment of associated physical processes and phenomena, including, for example, storm and cyclonic activity (Basu et al., 2018; Hochman et al., 2020; Raible et al., 2010) and water vapor transport (Sousa et al., 2020). Such an analysis is however beyond the scope of the present study.

As far as interannual-to-decadal climate variability in the Euro-Mediterranean region is concerned, comparison between the fraction of total variance explained by the modes in the *historical* and *ssp585* simulations indicate that, among the considered modes, EA is the predominant mode affecting Euro-Mediterranean

temperature both in the *historical* (explained variance estimated: ~13%) and in the *ssp585* ensemble (explained variance estimated: ~14%).

Concerning Euro-Mediterranean precipitation, there is an increase in the relevance of local processes with respect to large-scale dynamics and EAWR and SCA show a drop in explained variance from *historical* to *ssp585* simulations. Specifically, the simulations indicate a shift in predominance from SCA in the *historical* ensemble (explained variance estimated: ~11%) to NAO in the *ssp585* ensemble (explained variance estimated: ~12%). For the EAWR, this drop in covarying interannual variability especially regards precipitation over Southern Europe and the region north-east of the Caspian Sea (Figure S2 in Supporting Information S1).

In conclusion, our study demonstrates the capability of CMIP6 models to robustly simulate the observed patterns of Euro-Atlantic modes, including their associated climate impacts on the Euro-Mediterranean region. It also shows how climate mode's projections under a future changing climate could aid in the physical explanation of projected climate changes in this region.

Data Availability Statement

Data are available at: http://dx.doi.org/10.17632/j8jbt3wwsg.1.

Acknowledgments
The authors acknowledge the modeling groups listed in Table 1 for providing the model output for analysis, the WCRP's Working Group on Coupled Modelling (WGCM) for organizing the CMIP, and the Earth System Grid Federation (ESGF) for supporting the model data archive (https://esgf-data.dkrz.de/projects/esgf-dkrz/). The authors acknowledge also the Climate Prediction Center of the NOAA to provide the datasets for the North Atlantic teleconnections indices time-series, available at https://www.cpc.ncep.noaa.gov/data/teledoc/telecontents.shtml and the ECMWF for the 500 hPa geopotential height, sea-level pressure, temperature and precipitation datasets, available at https://apps.ecmwf.int/datasets/data/interim-full-daily/levtype=sfc/. The authors thank two anonymous reviewers for their helpful comments that contributed to improve the quality of the paper. Open Access Funding provided by Universita Ca' Foscari within the CRUI-CARE Agreement.

References

Barnston, A. G., & Livezey, R. E. (1987). Classification, seasonality and persistence of low-frequency atmospheric circulation patterns. *Monthly Weather Review*, *115*, 10832–11126. https://doi.org/10.1175/1520-0493(1987)115<1083:CSAPOL>2.0.CO;2

Basu, S., Zhang, X., & Wang, Z. (2018). Eurasian winter storm activity at the end of the century: A CMIP5 multi-model ensemble projection. *Earth's Future*, *6*(1), 61–70. https://doi.org/10.1002/2017ef000670

Bellucci, A., Gualdi, S., Scoccimarro, E., & Navarra, A. (2008). NAO-ocean circulation interactions in a coupled general circulation model. *Climate Dynamics*, *31*(7–8), 759–777. https://doi.org/10.1007/s00382-008-0408-4

Bi, D., Dix, M., Marsland, S., O'Farrell, S., Sullivan, A., Bodman, R., et al. (2020). Configuration and spin-up of ACCESS-CM2, the new generation Australian community climate and Earth system simulator coupled model. *Journal of Southern Hemisphere Earth Systems Science*, *70*(1), 225–251. https://doi.org/10.1071/ES19040

Bjerknes, J. (1964). Atlantic air-sea interaction. In *Advances in Geophysics* (Vol. 10, pp. 1–82). Elsevier. https://doi.org/10.1016/S0065-2687(08)60005-9

Boucher, O., Servonnat, J., Albright, A. L., Aumont, O., Balkanski, Y., Bastrikov, V., et al. (2020). Presentation and evaluation of the IPSL-CM6A-LR climate model. *Journal of Advances in Modeling Earth Systems*, *12*(7), https://doi.org/10.1029/2019MS00201

Bracegirdle, T. J., Lu, H., Eade, R., & Woollings, T. (2018). Do CMIP5 models reproduce observed low-frequency North Atlantic jet variability? *Geophysical Research Letters*, *45*(14), 7204–7212. https://doi.org/10.1029/2018GL078965

Bueh, C., & Nakamura, H. (2007). Scandinavian pattern and its climatic impact. *Quarterly Journal of the Royal Meteorological Society: A Journal of the Atmospheric Sciences, Applied Meteorology and Physical Oceanography*, *133*(629), 2117–2131. https://doi.org/10.1002/qj.173

Casado, M. J., & Pastor, M. A. (2012). Use of variability modes to evaluate AR4 climate models over the Euro-Atlantic region. *Climate Dynamics*, *38*(1), 225–237. https://doi.org/10.1007/s00382-011-1077-2

Cherchi, A., Fogli, P. G., Lovato, T., Peano, D., Iovino, D., Gualdi, S., et al. (2019). Global mean climate and main patterns of variability in the CMCC-CM2 coupled model. *Journal of Advances in Modeling Earth Systems*, *11*, 185–209. https://doi.org/10.1029/2018MS001369

Christidis, N., & Stott, P. A. (2015). Changes in the geopotential height at 500 hPa under the influence of external climatic forcings. *Geophysical Research Letters*, *42*(10), 10–798. https://doi.org/10.1002/2015GL066669

Cusinato, E., Zanchettin, D., Sannino, G., & Rubino, A. (2019). Mediterranean thermohaline response to large-scale winter atmospheric forcing in a high-resolution ocean model simulation. In I. Vilibić, K. Horvath, & J. L. Palau (Eds.), *Meteorology and climatology of the Mediterranean and black seas* (pp. 363–390). Birkhäuser. https://doi.org/10.1007/978-3-030-11958-4_22

Danabasoglu, G., Lamarque, J. F., Bachmeister, J., Bailey, D. A., DuVivier, A. K., Edwards, J., et al. (2020). The community earth system model version 2 (CESM2). *Journal of Advances in Modeling Earth Systems*, *12*. https://doi.org/10.1029/2019MS001916

Davini, P., & Cagnazzo, C. (2014). On the misinterpretation of the North Atlantic oscillation in CMIP5 models. *Climate Dynamics*, *43*(5–6), 1497–1511. https://doi.org/10.1007/s00382-013-1970-y

Dunne, J. P., Horowitz, L. W., Adcroft, A. J., Ginoux, P., Held, I. M., John, J. G., et al. (2020). The GFDL Earth system model version 4.1 (GFDL-ESM 4.1): Overall coupled model description and simulation characteristics. *Journal of Advances in Modeling Earth Systems*, *12*. https://doi.org/10.1029/2019MS002015

Eyring, V., Bony, S., Meehl, G. A., Senior, C. A., Stevens, B., Stouffer, R. J., & Taylor, K. E. (2016). Overview of the coupled model intercomparison project phase 6 (CMIP6) experimental design and organization. *Geoscientific Model Development*, *9*(5), 1937–1958. https://doi.org/10.5194/gmd-9-1937-2016

Frankignoul, C., Muller, P., & Zorita, E. (1997). A simple model of the decadal response of the ocean to stochastic wind forcing. *Journal of Physical Oceanography*, *27*, 1533–1546. https://doi.org/10.1175/1520-0485(1997)027<1533:asmotd>2.0.co;2

Hasselmann, K. (1976). Stochastic climate models part I. Theory. *tellus*, *28*(6), 473–485. https://doi.org/10.3402/tellusa.v28i6.11316

He, B., Bao, Q., Wang, X., Zhou, L., Wu, X., Liu, Y., et al. (2019). CAS FGOALS-f3-L model datasets for CMIP6 historical atmospheric model intercomparison project simulation. *Advances in Atmospheric Sciences*, *36*, 771–778. https://doi.org/10.1007/s00376-019-9027-8

Hintze, J. L., & Nelson, R. D. (1998). Violin plots: A box plot-density trace synergism. *The American Statistician*, *52*(2), 181–184. https://doi.org/10.1080/00031305.1998.10480559

Hochman, A., Alpert, P., Kunin, P., Rostkier-Edelstein, D., Harpaz, T., Saaroni, H., & Messori, G. (2020). The dynamics of cyclones in the twenty-first century: The Eastern Mediterranean as an example. *Climate Dynamics*, *54*(1), 561–574. https://doi.org/10.1007/s00382-019-05017-3

Hoerling, M. P., Hurrell, J. W., & Xu, T. (2001). Tropical origins for recent North Atlantic climate change. *Science*, *292*(5514), 90–92. https://doi.org/10.1126/science.1058582

Hurrell, J. W., Kushnir, Y., Ottersen, G., & Visbeck, M. (2003). An overview of the North Atlantic oscillation. *Geophysical Monograph-American Geophysical Union*, *134*, 1–36. https://doi.org/10.1029/134GM01

Krishnan, R., Swapna, P., Vellore, R., Narayanasetti, S., Prajeesh, A. G., Dey Choudhury, A., et al. (2019). The IITM Earth system model (ESM): Development and future roadmap. In D. Randall, J. Srinivasan, R. Nanjundiah, & P. Mukhopadhyay (Eds.), *Current trends in the Representation of physical processes in weather and climate models* (pp. 183–195). Springer. https://doi.org/10.1007/978-981-13-3396-5_9

Lee, W. L., Wang, Y. C., Shiu, C. J., Tsai, I. C., Tu, C. Y., Lan, Y. Y., et al. (2020). Taiwan Earth system model version 1: Description and evaluation of mean state. *Geoscientific Model Development*, *13*(9), 3887–3904. https://doi.org/10.5194/gmd-13-3887-2020

Li, L., Yu, Y., Tang, Y., Lin, P., Xie, J., Song, M., et al. (2020). The flexible global ocean-atmosphere-land system model grid-point version 3 (FGOALS-G3): Description and evaluation. *Journal of Advances in Modeling Earth Systems*, *12*. https://doi.org/10.1029/2019MS002012

Lim, Y. K. (2015). The East Atlantic/West Russia (EA/WR) teleconnection in the North Atlantic: Climate impact and relation to Rossby wave propagation. *Climate Dynamics*, *44*(11-12), 3211–3222.

Marshall, J., Kushnir, Y., Battisti, D., Chang, P., Dickson, R., Hurrell, J., et al. (2001). North Atlantic climate variability: Phenomena, impacts and mechanisms. *International Journal of Climatology*, *21*, 1863–1898. https://doi.org/10.1002/joc.693

Massonnet, F., Ménégoz, M., Acosta, M., Yepes-Arbós, X., Exarchou, E., & Doblas-Reyes, F. J. (2020). Replicability of the EC-Earth3 Earth system model under a change in computing environment. *Geoscientific Model Development*, *13*(3), 1165–1178. https://doi.org/10.5194/gmd-13-1165-2020

Müller, W. A., Jungclaus, J. H., Mauritsen, T., Baehr, J., Bittner, M., Budich, R., et al. (2018). A higher-resolution version of the Max Planck Institute Earth System Model (MPI-ESM1.2-HR). *Journal of Advances in Modeling Earth Systems*, *10*, 1383–1413. https://doi.org/10.1029/2017MS001217

Ning, L., & Bradley, R. S. (2016). NAO and PNA influences on winter temperature and precipitation over the eastern United States in CMIP5 GCMs. *Climate Dynamics*, *46*(3–4), 1257–1276. https://doi.org/10.1007/s00382-015-2643-9

Perlwitz, J., & Graf, H.-F. (1995). The statistical connection between tropospheric and stratospheric circulation of the northern hemisphere in winter. *Journal of Climate*, *8*(10), 2281–2295. https://doi.org/10.1175/1520-0442(1995)008<2281:TSCBTA>2.0.CO;2

Raible, C. C., Lehner, F., González-Rouco, J. F., & Fernández-Donado, L. (2014). Changing correlation structures of the Northern Hemisphere atmospheric circulation from 1000 to 2100 AD. *Climate of the Past*, *10*, 537–550. https://doi.org/10.5194/cp-10-537-2014

Raible, C. C., Stocker, T. F., Yoshimori, M., Renold, M., Beyerle, U., Casty, C., & Luterbacher, J. (2005). Northern hemispheric trends of pressure indices and atmospheric circulation patterns in observations, reconstructions, and coupled GCM simulations. *Journal of Climate*, *18*(19), 3968–3982. https://doi.org/10.1175/JCLI3511.1

Raible, C. C., Ziv, B., Saaroni, H., & Wild, M. (2010). Winter synoptic-scale variability over the Mediterranean Basin under future climate conditions as simulated by the ECHAM5. *Climate Dynamics*, *35*(2–3), 473–488. https://doi.org/10.1007/s00382-009-0678-5

Rong, X. Y., Li, J., Chen, H. M., Xin, Y. F., Su, J. Z., Hua, L. J., & Zhang, Z. Q. (2019). Introduction of CAMS-CSM model and its participation in CMIP6. *Climate Change Research*, *15*(5), 540–544. https://doi.org/10.12006/j.issn.1673-1719.2019.186

Schneider, E. K., Bengtsson, L., & Hu, Z. Z. (2003). Forcing of northern hemisphere climate trends. *Journal of the Atmospheric Sciences*, *60*(12), 1504–1521. https://doi.org/10.1175/1520-0469(2003)060<1504:FONHCT>2.0.CO;2

Seland, Ø., Bentsen, M., Olivié, D., Toniazzo, T., Gjermundsen, A., GraffDebernard, L. S. J. B., et al. (2020). Overview of the Norwegian Earth System Model (NorESM2) and key climate response of CMIP6 DECK, historical, and scenario simulations. *Geoscientific Model Development*, *13*(12), 6165–6200. https://doi.org/10.5194/gmd-13-6165-2020

Semmler, T., Danilov, S., Gierz, P., Goessling, H. F., Hegewald, J., Hinrichs, C., et al. (2020). Simulations for CMIP6 with the AWI climate model AWI-CM-1-1. *Journal of Advances in Modeling Earth Systems*, *12*, e2019MS002009. https://doi.org/10.1029/2019MS002009

Shaw, T. A., & Perlwitz, J. (2013). The life cycle of northern hemisphere downward wave coupling between the stratosphere and troposphere. *Journal of Climate*, *26*(5), 1745–1763. https://doi.org/10.1175/JCLI-D-12-00251.1

Song, Z. Y., Bao, Y., & Qiao, F. L. (2019). Introduction of FIOESM v2.0 and its participation plan in CMIP6 experiments. *Climate Change Research*, *15*, 558–565. https://doi.org/10.12006/j.issn.1673-1719.2019.033

Sousa, P. M., Ramos, A. M., Raible, C. C., Messmer, M., Tomé, R., Pinto, J. G., & Trigo, R. M. (2020). North Atlantic integrated water vapor transport—From 850 to 2100 CE: Impacts on western European rainfall. *Journal of Climate*, *33*(1), 263–279. https://doi.org/10.1175/jcli-d-19-0348.1

Stephenson, D. B., Pavan, V., Collins, M., Junge, M. M., & Quadrelli, R. (2006). North Atlantic Oscillation response to transient greenhouse gas forcing and the impact on European winter climate: A CMIP2 multi-model assessment. *Climate Dynamics*, *27*(4), 401–420.

Swart, N. C., Cole, J. N. S., Kharin, V. V., Lazare, M., Scinocca, J. F., Gillett, N. P., et al. (2019). The Canadian Earth System Model version 5 (CanESM5.0.3). *Geoscietific Model Development*, *12*(11), 4823–4873. https://doi.org/10.5194/gmd-12-4823-2019

Tatebe, H., Ogura, T., Nitta, T., Komuro, Y., Ogochi, K., Takemura, T., et al. (2019). Description and basic evaluation of simulated mean state, internal variability, and climate sensitivity in MIROC6. *Geoscientific Model Development*, *12*(7), 2727–2765. https://doi.org/10.5194/gmd-12-2727-2019

Thompson, D. W., Lee, S., & Baldwin, M. P. (2003). Atmospheric processes governing the northern hemisphere annular mode/North Atlantic oscillation. *Geophysical Monograph-American Geophysical Union*, *134*, 81–112. https://doi.org/10.1029/134GM05

Volodin, E. M., Mortikov, E. V., Kostrykin, S. V., Galin, V. Y., Lykossov, V. N., Gritsun, A. S., et al. (2018). Simulation of the modern climate using the INM-CM48 climate model. *Russian Journal of Numerical Analysis and Mathematical Modelling*, *33*(6), 367–374. https://doi.org/10.1515/rnam-2018-0032

Wallace, J. M., & Gutzler, D. S. (1981). Teleconnections in the geopotential height field during the Northern Hemisphere winter. *Monthly Weather Review*, *109*(4), 784–812. https://doi.org/10.1175/1520-0493(1981)109<0784:TITGHF>2.0.CO;2

Wang, X., Li, J., Sun, C., & Liu, T. (2017). NAO and its relationship with the Northern Hemisphere mean surface temperature in CMIP5 simulations. *Journal of Geophysical Research: Atmospheres*, *122*(8), 4202–4227. https://doi.org/10.1002/2016JD025979

Welch, P. (1967). The use of the fast Fourier transform for the estimation of power spectra: A method based on time averaging over short, modified periodograms. *IEEE Transactions on Audio and Electroacoustics*, *15*(2), 70–73. https://doi.org/10.1109/TAU.1967.1161901

Woollings, T., Hoskins, B., Blackburn, M., & Berrisford, P. (2008). A new Rossby wave-breaking interpretation of the North Atlantic Oscillation. *Journal of the Atmospheric Sciences*, *65*(2), 609–626. https://doi.org/10.1175/2007JAS2347.1

Wu, T., Lu, Y., Fang, Y., Xin, X., Li, L., Li, W., et al. (2019). The Beijing climate center climate system model (BCC-CSM): The main progress from CMIP5 to CMIP6. *Geoscientific Model Development*, *12*(4), 1573–1600. https://doi.org/10.5194/gmd-12-1573-2019

Wyser, K., Noije, T. V., Yang, S., Hardenberg, J. V., O'Donnell, D., & Döscher, R. (2020). On the increased climate sensitivity in the EC-Earth model from CMIP5 to CMIP6. *Geoscientific Model Development*, *13*(8), 3465–3474. https://doi.org/10.5194/gmd-13-3465-2020

Yukimoto, S., Kawai, H., Koshiro, T., Oshima, N., Yoshida, K., Urakawa, S., et al. (2019). The Meteorological Research Institute Earth System Model version 2.0, MRI-ESM2. 0: Description and basic evaluation of the physical component. *Journal of the Meteorological Society of Japan. Series II*, *97*, 931–965. https://doi.org/10.2151/jmsj.2019-051

Zanchettin, D., Bothe, O., Rubino, A., & Jungclaus, J. H. (2016). Multi-model ensemble analysis of Pacific and Atlantic SST variability in unperturbed climate simulations. *Climate Dynamics*, *47*, 1073–1090. https://doi.org/10.1007/s00382-015-2889-2

Zanchettin, D., Rubino, A., Traverso, P., & Tomasino, M. (2008). Impact of variations in solar activity on hydrological decadal patterns in northern Italy. *Journal of Geophysical Research*, *113*, D12102. https://doi.org/10.1029/2007JD009157

Zanchettin, D., Rubino, A., Traverso, P., & Tomasino, M. (2009). Teleconnections force interannual-to-decadal tidal variability in the Lagoon of Venice (northern Adriatic). *Journal of Geophysical Research*, *114*(D7). https://doi.org/10.1029/2008JD011485

Zanchettin, D., Timmreck, C., Graf, H. F., Rubino, A., Lorenz, S., Lohmann, K., et al. (2012). Bi-decadal variability excited in the coupled ocean–atmosphere system by strong tropical volcanic eruptions. *Climate Dynamics*, *39*(1), 419–444. https://doi.org/10.1007/s00382-011-1167-1

Ziehn, T., Chamberlain, M. A., Law, R. M., Lenton, A., Bodman, R. W., Dix, M., et al. (2020). The Australian earth system model: ACCESS-ESM1.5. *Journal of Southern Hemisphere Earth Systems Science*, *70*(1), 193–214. https://doi.org/10.1071/ES19035